GEOPHYSICAL RESEARCH LETTERS, VOL. ???, XXXX, DOI:10.1029/,

The topography of inland deltas: observations, modeling, experiments

H.J. Seybold,[1] P. Molnar,[2] D. Akca,[4] M. Doumi,[3] M. Cavalcanti Tavares,[5]

T. Shinbrot,[3] J.S. Andrade Jr.,[5] W. Kinzelbach,[2] H.J. Herrmann[1,5]

H. J. Seybold, Computational Physics, IfB, ETH Zurich, 8093 Zurich, Switzerland (hseybold@ethz.ch)

[1] Computational Physics for Engineering

The topography of inland river deltas is influenced by the water-sediment balance in the distributary channel system and the local evaporation and seepage rates. We apply a reduced complexity model to simulate an inland delta and compare the results with the Okavango Delta and with a laboratory experiment. We show that water loss through evapotranspiration and infiltration in inland deltas produces fundamentally different dynamics of water and sediment transport than coastal deltas, especially vis a vis deposition associated with expansion-contraction dynamics at the channel head. These dy-

Materials, IfB, ETH Zurich, 8093 Zurich, Switzerland

[2] Institute of Environmental Engineering, IfU, ETH Zurich 8093 Zurich, Switzerland

[3] Department of Biomedical Engineering, Rutgers University, Piscataway, NJ 08854, USA

[4] Institute of Geodesy and Photogrammetry, ETH Zurich 8093 Zurich, Switzerland

[5] Departamento de Física, Universidade Federal do Ceará, 60451-970 Fortaleza , Ceará, Brasil

namics lead to a systematic decrease in the mean topographic slope of the inland delta with distance from the apex that follows a power law with exponent $\alpha = -0.69$ for both simulation and experiment. In coastal deltas, on the contrary, the slope increases toward the end of the deposition lobe.

1. Introduction

Inland deltas like the Okavango and coastal deltas like the Mississippi are morphologically distinct because their deposition patterns are influenced by different dominant fluvial processes. Coastal deltas are dominated by wave and tide action and coastal currents that separate the subaerial and subaqueous parts of the delta lobes. Inland deltas, on the other hand, experience none of these flows, but are dominated by evapotranspiration, infiltration, and the growth of bank- and island-stabilizing vegetation.

Inland deltas are less well studied than their coastal counterparts. We investigate geomorphological features of inland deltas, which we compare with coastal ones. We focus on the Okavango Delta as a case study, and we compare its topography with computational simulations using a new reduced complexity model [*Seybold et al.*, 2007, 2009], as well as a small-scale laboratory experiment.

As we will explain, the geomorphological evolution of the Okavango Delta surface is strongly influenced by the dynamics and transport capabilities of its constituent channels, where interactions with the local slope and properties of the alluvium and surface vegetation play an essential role. Additionally, tectonic movement of the surface can play a role that we briefly discuss.

In recent years several field measurements and hydrological models of the Okavango Delta have been produced, including measurements of sediment rating in the delta channels and groundwater fluxes [*Bauer et al.*, 2004; *McCarthy*, 2006; *Gumbricht et al.*, 2005; *Brunner et al.*, 2007]. The models constructed so far, however, are only capable of short term forecasting, with management horizons of maximally 50 years.

In order to describe longer-term dynamics of sediment transport, and consequent development of the delta, new models must be developed that reduce the complexity of the hydrological and sedimentary equations while maintaining the essential physics [*Brasington and Richards*, 2007; *Crave and Davy*, 2001]. In particular, the model proposed by *Seybold et al.* [2007] has proven to describe coastal delta formation successfully, and we extend this model here to include evaporative water loss and seepage for the study of morphogenesis of inland deltas like the Okavango.

To study the processes leading to this rich geomorphology, we present computational model accompanied by a laboratory-scale flume experiment. Flume experiments on delta formation have been carried out in several laboratories, notably the Earthscape Experiment laboratory in St. Anthony Falls and the Exxon Mobil laboratories [*Hoyal and Sheets*, 2009; *Martin et al.*, 2009]. Also recently, the formation of alluvial fans caused by rapid water release has been studied by *Kraal et al.* [2008]. However, experimental work on inland deltas including evaporation is new. We use these experiments as a verification for the modeling and as a tool to understand the interplay between the dominant sedimentary processes.

The paper is organized as follows: first we show how the computational model of *Seybold et al.* [2007, 2009] was modified to include evaporation. Then we describe our experiment mimicking inland delta formation. We then discuss results and analysis in two subsections. First we compare the model results with topographic data of the Okavango, topological structure of the channel system and the influence of evaporation on the sedimentation process. Second, we study the delta slope distributions in both modeled and observed data and discuss the differences.

2. Computational Modeling

To simulate inland delta formation, we extended the model of *Seybold et al.* [2007, 2009] to include evaporation and seepage in the conservation equation for water mass, as follows. The landscape is discretized on a square grid where the elevation of the topography H_i and the absolute water level V_i are defined on the nodes. The water flux I_{ij} on a bond is related to the average water depth σ_{ij} and the pressure drop $V_i - V_j$ by the following relation:

$$I_{ij} = \underbrace{\left(\frac{V_i - H_i}{2} + \frac{V_j - H_j}{2} \right)}_{=\sigma_{ij}} (V_i - V_j). \tag{1}$$

Conservation of water flows entering and leaving node i is given by:

$$V_i = V_i' + \delta t \sum_{N.N.} (I_{ij} + E_i) = 0, \tag{2}$$

where E_i defines the loss of water due to evaporation or infiltration and the sum runs over the von Neumann neighborhood of a given cell. The evaporation rate is modeled by the following phenomenological formula

$$E_i = d_i \hat{E} \tag{3}$$

where $\hat{E}$ defines the maximum evapotranspiration rate and so determines how far the delta progrades into the domain. The increase of seepage in distal parts of the delta is modeled by the normalized distance of the cell from the inlet, d_i.

Boundary and initial conditions are needed to close the problem. The landscape is initialized with an inclined plane, distorted by random perturbations. Open boundary conditions are applied at all boundaries except in the nodes closest to the inlet where no-flow boundaries are applied to keep the water flowing into the domain. Water and sediment are injected into the system by defining an input flux I_0 of water and sediment s_0 at an entrance node. The landscape is initialized with a given water level below the ground, and runoff is produced when the water level exceeds the surface. The sedimentation-erosion rate dS_{ij} is modeled by a phenomenological deposition-erosion law with a common constant c for erosion and deposition [*Seybold et al.*, 2009]. The deposition-erosion law depends only on the magnitude of the flow,

$$dS_{ij} = c(I^\star - |I_{ij}|), \tag{4}$$

and a threshold $I^\star$ which determines whether erosion or deposition occurs between nodes i and j. After the sedimentation-/erosion process the sediment $J_g es$ is distributed to the outflow directions according to their relative magnitudes of the corresponding water flux, e.g. $J_{kl} = I_{kl}/\sum_i I_{il}$. Sediment transport and topography update is done in the same way as in *Seybold et al.* [2009].

Two types of channel ends need to be included in inland deltas: newly forming channels where $\mathrm{d}I = I(t + \delta t) - I(t) > 0$ do not show sedimentation at the front, and channels that are drying with high deposition rates at their terminal ends. These are included by distinguishing ends with $\mathrm{d}I > 0$ and $\mathrm{d}I < 0$. If $\mathrm{d}I < 0$, deposition is applied according to Eq.4, while if $\mathrm{d}I > 0$, no deposition is applied in the final node of a channel end.

3. Experimental Modeling

To validate the computations, we performed a laboratory-scale flume experiment including evaporation and seepage. Our experiment consists of a $1m$ by $1m$ aluminum basin that is fixed at an inclination of about 6 degrees running along the basin diagonal. An initial surface is created using a uniformly sloped sediment layer with an height of $5cm$ at the inlet diminishing to zero over about $1.1m$ (Fig. 1).

As sediment, we use crushed glass with diameter 50 to 120 microns, with a bulk density of $\varrho = 2.2g/cm^3$. The sediment is continuously mixed with water by a marine-type impeller in an upstream tank, and is injected steadily into the basin using a peristaltic pump. The volumetric sediment concentration was approximately 0.05 and the inflow was $1000ml/h$. Water is continuously pumped out of the basin at the bottom so that no standing water accumulates. Water is evaporated by an array of fifteen $300W$ heat lamps that are fixed $15cm$ above the surface.

The experiment was run as follows: a water/sediment mixture was injected into the flume over 45 minutes, followed drying over 2:15 hours. In the following we will call one period of injection and drying an "epoch", where epoch 0 stands for the initial condition. A photo of the initial setup is shown in Fig. 1b. After complete drying, the surface topography is scanned using a Breukmann OptoTOP-SE 3D scanner. Complete drying is necessary to avoid specular reflections produced by wet Sand that would disturb the scanning procedure. The scanning technique is based on a stereoscopic measurement, in which regular fringes are projected onto the surface and the stripes' deformation is measured using a CCD camera. From the deformation of these lines the topography can be reconstructed with an accuracy of 100 microns [*Burke et al.*, 2002; *Akca et al.*, 2007]. Due to the limited field-of view of the scanner ($40cm \times 31cm$), several scans are combined into a co-registered mosaic of the entire surface, using a least square matching method described elsewhere *Gruen and Akca* [2005]. We use an invariant reference point outside of the sedimentation domain to co-register the different sediment layers so that we can obtain temporal and spatial distributions of sediment during the experiment.

The total deposited volume of each epoch including pore space can be obtained by subtracting the co-registered surfaces of two successive topography scans. For the four injection periods we obtained $V_{0,1} = 573cm^3$, $V_{1,2} = 904cm^3$, $V_{2,3} = 614cm^3$ and $V_{3,4} = 740cm^3$, where the indices denote the epochs before and after the deposition run.

To compare with the wet delta case, we remove the heat lamps and change the boundary conditions at the downstream end of the flume to preserve a constant water level, while keeping the other parameters unchanged.

Although the experimental results cannot be directly compared with natural Deltas due to large scale variations, the deposition processes and the resulting patterns are similar to those observed in nature.

4. Analysis of inland delta formation

4.1. Modeling and observations of delta channels

Visually, the computational inland delta model produced deposition structures and channels similar to natural deltas. The topological similarities of the different delta channel systems are quantified by estimating the fractal dimension of simulated and observed networks with the box counting technique [*Feder*, 1989; *Turcotte*, 1997].

A least squares fit of a power law, $N \sim s^{-D}$ to the data yields a fractal dimension of $D = 1.85 \pm 0.05$ for the Okavango Delta, as compared with the simulation result of $D = 1.84 \pm 0.05$. The pattern of the flooded area of the Okavango was extracted through the vegetation by a combined analysis of high resolution aerial photos from GoogleEarth™ and NOAA satellite measurements. The added processes of evaporation and infiltration lead to complex dynamics of channel extension by erosion and contraction due to deposition at the channel heads during low flows which we could not observe in wet deltas. Furthermore, the model reproduces the development of bank levees by lateral deposition on channel margins (Fig. 1c). The natural formation of bank levees by overbank deposition occurs in the Okavango and in many natural dryland rivers [*McCarthy et al.*, 1988] due to processes such as vegetation that are notoriously difficult to simulate. This riparian vegetation [*McCarthy et al.*, 1992] modulates overbank deposition in the Okavango delta and affects not only deposition but also evapotranspiration and infiltration rates. In the model, natural levee formation is due to lateral topographic gradients and the balance of sediment supply and transport.

4.2. Delta slope distributions

A useful topographic metric to quantify the shape of a delta is the mean slope as a function of downstream distance from the delta apex. We define the mean topographic slope $S(d)$ averaged over circular arcs at a distance $[d, d + \mathrm{d}r]$ from the delta apex. In order to compare the different observed, numerical and experimentally modeled slopes, we normalize the results with the overall spatial mean,

$$S(d) = \frac{1}{\langle S \rangle} \langle S \rangle_{d+\mathrm{d}r} . \tag{5}$$

The averages are computed over a spatial domain which contains the whole delta surface. $S(d)$ is a useful measure of the delta form for two reasons. First, it is an integral measure (over the whole domain) of the processes of deposition in space at an equal distance from the apex. Second, topographic slope is a fundamental variable for sediment transport in transport capacity-limited conditions such as delta distributary channels.

Most landscape evolution models relate sediment transport capacity Q_s and the erosion/deposition rate to upstream drainage area A and local slope $Q_s \sim A^m S^n$, where m and n are fundamental exponents which reflect the erodibility of the surface and the erosivity of the flow (e.g., *Davy et al.* [2009]; *Niemann et al.* [2001]. Delta distributary systems are conduits without an increase in drainage area, and it is therefore reasonable to assume that the specific sediment transport rate will scale as,

$$Q_s \sim S^n. \tag{6}$$

Therefore, $S(d)$ is an indication of the radial distribution of the potential sediment transporting capacity of the delta system, where the specific water q and sediment Q_s transport rate and the downstream change in total distributary channel width $W(d)$ together determine the total sediment transporting capacity of the system.

In order to compare Okavango and simulated topography more directly, we rescaled the horizontal extents of the simulation to fit the experimental domain. A comparison of $S(d)$ for the modeled surface, the experiment and the Okavango DEM surface [*Gumbricht et al.*, 2005] is shown in Fig. 2.

The modeled surface shows a gradual decrease in $S(d)$ downstream as the sediment transporting capacity in smaller (but more numerous) channels decreases, and the delta becomes flatter as a consequence. Furthermore the transport capacity decreases due to the loss of transporting water by evaporation and seepage. Local variations may be associated with the varying heads of individual distributary channels which may be actively eroding and so can be expected to have a higher local slope. Fig. 2a displays the statistical average over nine simulation runs with the same evaporation rate and boundary conditions, but different random perturbations to the initial surface. The errorbars indicate the statistical variability. The parameters for this simulation have been chosen to be $I_0 = 1 \times 10^{-3}$, $I^\star = -7.5 \times 10^{-6}$, $s_0 = 0.0025$, $c = 0.1$ [*Seybold et al.*, 2009], and the evaporation rate in this case is set to $\hat{E} = 5 \times 10^{-8}$.

As shown in the inset of Fig. 3, the local slopes obtained from the dry delta experiments as well as from model simulations clearly follow power-law behavior, $S = a(d - d_0)^\alpha$. As one would expect, the least-squares fit to the data sets of this function indicates that both the a and d_0 depend on the particular experimental/simulation conditions. In particular, the parameter d_0 assumes negative values in the two cases, which is consistent with the physical condition of divergence-free slope profiles for positive distances. More strikingly, however, is the fact that we obtain identical power-law exponents $\alpha \approx -0.69$ for experimental data and model simulations.

As shown in the main plot of Fig.3, this is corroborated by the data collapse obtained by rescaling S to $S^* = S/a$ and plotting it against $d^* = d - d_0$.

The Okavango surface shows a more complex behavior affected strongly by local geology and tectonics. During the first $100km$ the Okavango is confined between the fault lines forming the a confined area, called the Panhandle.

Outside the Panhandle the delta surface is almost totally flat with only small local variability around the constant slope of the fan. The increase in mean slope at the bottom end of the delta is a consequence of the Kunyere and Thamalakane fault lines.

The downstream distribution of slope also highlights the fundamental difference between wet (coastal) and dry (inland) deltas. The Mississippi Delta Balize Lobe profile from bathymetric data in [*Seybold et al.*, 2009; *Divins and Metzger*, 2006] shows that in coastal deltas the mean slope increases downstream as the distributary channels enter the ocean and sediment deposition becomes limited by the settling velocity of particles and their advection by currents and tides (Fig. 4). In the DEM data of the Balize Lobe the slope is increasing exponentially with a characteristic inverse length of $\tau = 0.026$ at the head of the delta (Fig. 4b). Furthermore it can be seen that with time the Mississippi River has adjusted the average slope of its fluvially accessible area to the optimal transport capacity of the stream and therefore we observe a constant slope on the coastal plain.

A strongly increasing slope toward the end of the lobes is also observed in the reduced complexity model simulations of *Seybold et al.* [2009] but the functional behavior of the increase at the delta head could not be verified from the data (Fig.4a). The average slope of the birdfoot delta simulation presented in Fig. 4a is averaged over 5 different samples with the same set of parameters but different random noise in the initial conditions of the surface. The parameters have been chosen similar to *Seybold et al.* [2009], namely $I_0 = 0.00017$, $I^\star = -4 \times 10^{-6}$, $s_0 = 0.00025$, $c = 0.1$. In the simulation the river first adjusts the slope imposed by the initial conditions to its transport capacity (Fig. 4a-I) until it flows at an almost constant slope in the newly formed lobe (Fig. 4a-II between $d = 80 - 120km$). The decay of the slope in the initial part can be fitted by a power law with an exponent around $\alpha \approx -0.4$.

The same phenomenon is observed in the experiment (Fig. 4c). We find a decreasing slope in the initial part of the flume where the stream adjusts the base slope due to erosion and deposition (Fig. 4c-I). In a middle part (Fig. 4c-II), the coastal slope is adjusted to the stream transport capacity and this is constant over a certain range. Toward the head of the delta the slope increases strongly again and then drops to the base slope of the basin (Fig. 4c-III). Although the average slope for the experiment is noisy, the three parts can be identified. The functional behavior of the increasing part could not be determined from the data. We have removed the very initial part of the flume from the average slope calculation because this section is strongly influenced by details associated with the slurry injection.

5. Conclusions

In this paper we adjusted and applied a reduced complexity model which was originally developed for coastal deltas [*Seybold et al.*, 2009], to an inland delta, using elevation- and slope-based metrics to describe its shape and change. The Okavango Delta was used as a reference to compare with the model, together with a small-scale laboratory experiment to verify the modeling results and understand the time evolution of the delta system.

The chief finding of this study is that water loss through evapotranspiration and infiltration in an inland delta combine to produce a fundamentally different dynamics of water and sediment transport compare to coastal deltas. In particular, the expansion-contraction dynamics at the channel heads and the deposition associated with these dynamics lead to a consistent decrease in the mean topographic slope in inland deltas with distance from the apex. The decrease of the slope in the experimental as well as the modeled systems shows a clear power law behavior. By rescaling the variables it is possible to collapse the two curves on a single power law with exponent $\alpha = -0.69$.

Inland deltas are transport capacity-limited systems. The systematically decreasing topographic slope from the delta apex is indicative of a drop in specific sediment transporting capacity along the delta channel system, which, combined with the number and width of the distributary channels, governs the sediment transport capacity of the delta as a whole and the sedimentation within the fan. This simple topographic measure also highlights the difference between inland and coastal deltas insofar as topographic slope in the latter case increases dramatically at the land-ocean interphase.

Acknowledgments. This work was funded by the Swiss National Foundation Grant NF20021-116050/1.

References

Akca, D., F. Remondino, D. Novàk, T. Hanusch, G. Schrotter, and A. Gruen (2007), Performance evaluation of a coded structured light system for cultural heritage applications, in *Videometrics IX, Proc. of SPIE-IS&T Electronic Imaging*, pp. 64,910V–1–12, San Jose (California), USA.

Bauer, P., G. Thabeng, F. Stauffer, and W. Kinzelbach (2004), Estimation of the evapotranspiration-rate from diurnal groundwater level fluctuations in the okavango delta, botswana, *Journal of Hydrology*, *288*(3-4), 344–355.

Brasington, J., and K. Richards (2007), Reduced-complexity, physically-based geomorphological modelling for catchment and river management, in *Geomorphology, special* *issue*, vol. 90, pp. 171–177, Elsevier, doi:10.1016/j.geomorph.2006.10.028.

Brunner, P., H. Hendricks Franssen, L. Kgotlhang, P. Bauer-Gottweiler, and W. Kinzelbach (2007), Howremote sensing contribute to ground water modeling, *Hydrogeol. J.*, *15*(1), 5–18.

Burke, J., T. Bothe, W. Osten, , and C. Hess (2002), Reverse engineering by fringe projection, *Interferometry XI: Applications, SPIE*, *4778*, 312–324.

Crave, A., and P. Davy (2001), A stochastic "precipiton" model for simulating erosion/sedimentation dynamics, *Computers & Geosciences*, *27*(7), 815 – 827, doi:DOI: 10.1016/S0098-3004(00)00167-9.

Davy, P., , and D. Lague (2009), Fluvial erosion/transport equation of landscape evolution models revisited, *J. Geophys. Res.*, *114*(F03007), doi:doi:10.1029/2008JF001146.

Divins, D., and D. Metzger (2006), Coastal relief model, Central Gulf of Mexico Grids.

Feder, J. (1989), *Fractals*, 4 ed., Plenum Press, New York.

Gruen, A., and D. Akca (2005), Least squares 3d surface and curve matching, *Journal of Photogrammetry and Remote Sensing*, *59*(3), 151–174.

Gumbricht, T., T. S. McCarthy, and P. Bauer (2005), Micro-topography of the okavango delta wetlands, *Earth. Surf. Proc. Land.*, *30*, 27–29.

Hoyal, D., and B. Sheets (2009), Morphodynamic evolution of cohesive experimental deltas, *J. Geophys. Res. Earth-Surface*, *114*(F02009), 78–89, doi: 10.1029/2007JF000882.

Kraal, E., M. van Dijk, G. Postma, and M. Kleinhans (2008), Martian stepped-delta formation by rapid water release, *Nature*, *451*, 973–976.

Martin, J., B. Sheets, C. Paola, and D. Hoyal (2009), Influence of steady base-level rise on channel mobility, shoreline migration, and scaling properties of cohesive experimental delta, *J. Geophys. Res.*, *114* (F03017), doi:doi:10.1029/2008JF001142.

McCarthy, T. (2006), Groundwater in the wetlands of the Okavango Delta, Botswana, and its contribution to the structure and function of the ecosystem, *J. Hydrol.*, *320*, 264–282.

McCarthy, T. S., K. H. Rogers, I. G. Stanistreet, W. N. Ellery, B. Cairncross, K. Ellery, and T. Gorbicki (1988), Features of channel margins in the okavango delta, *Palaeoecol. Africa*, *19*, 3–14.

McCarthy, T. S., W. N. Ellery, and I. G. Stanistreet (1992), Avulsion mechanisms on the okavango fan, botswana - the control of a fluvial system by vegetation, *Sedimentology*, *39* (5), 779–795.

Niemann, J., N. Gasparini, and G. Tucker (2001), A quantitative evaluation of playfair's law and its use in testing long-term stream erosion models, *Earth. Surf. Proc. Land.*, *26* (12), 1317–1332.

Seybold, H., J. Andrade Jr., and H. J. Herrmann (2007), Modeling river delta formation, *Proc. Natl. Acad. Sci. USA*, *104* (43), 16,804–16,809.

Seybold, H., P. Molnar, H. Singer, J. Andrade Jr., H. Herrmann, and W. Kinzelbach (2009), Simulation of birdfoot delta formation with application to the Mississippi Delta, *J. Geophys. Res. Earth-Surface*, *114* (F03012), doi:doi:10.1029/2009JF001248.

Turcotte, D. (1997), *Fractals and chaos in geology and geophysics*, Camebridge University Press.

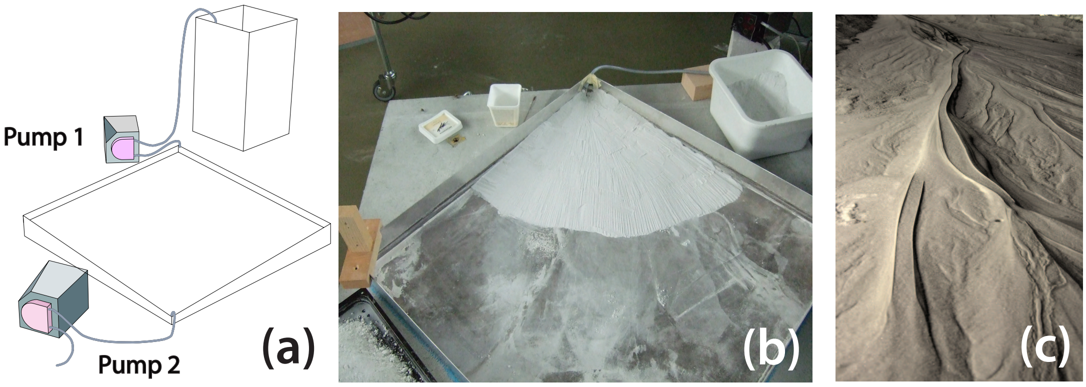

Figure 1. Sketch of the experimental setup (a). Water and sediment are fed from a container where the sediment is kept in suspension using an electric mixer. The sediment-water suspension then is injected into the basin using a peristaltic pump (Ismatec ecoline, pump 1). At the end of the flume remaining water is pumped out of the basin (pump 2). (b) Initial condition of the experiment. The flume is mounted on an inclined concrete base and an initial conical landscape of sediment is created in the first third of the domain. (c) The photo shows the deposition pattern of the dry delta experiment after several cycles of delta formation with braiding streams and levees confining the channels.

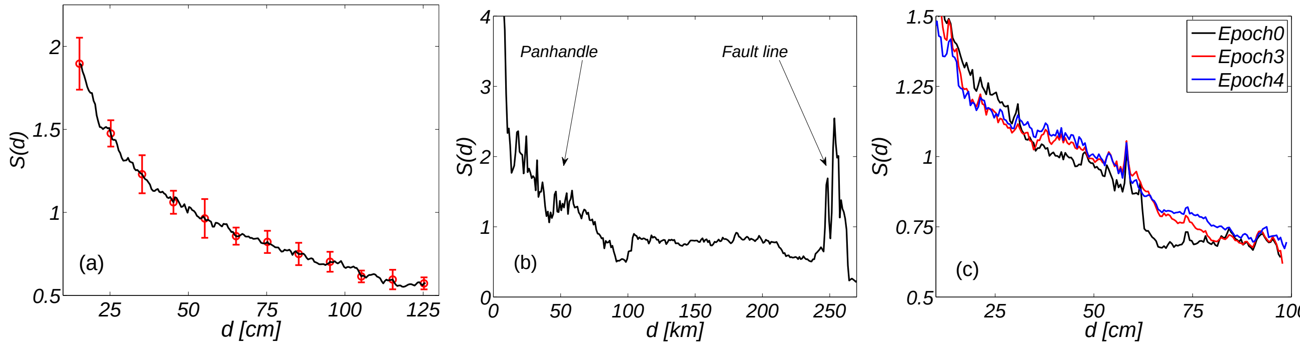

Figure 2. Plot of the slope $S(d)$ (a) for the simulation averaged over 9 samples, the errorbars indicate the statistical error, (b) the Okavango derived from DEM data and (c) the experiment (initial condition, epoch 3 and 4). Both experiment and simulation show a similar decreasing slope with distance to the apex. The detailed analysis of the decrease is presented in Fig. 3.

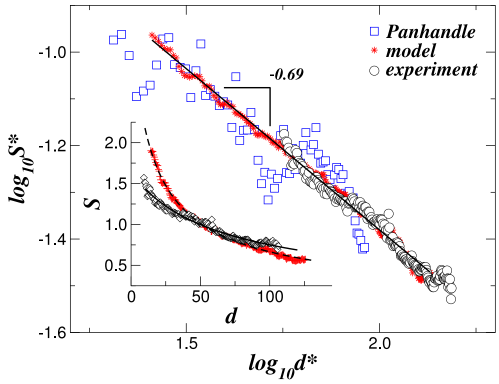

Figure 3. The inset shows the decay of the slope for both experiment (epoch 5, black diamonds) and model (red crosses) in dry deltas together with the corresponding least-square fits of a power-law of the form $S = a(d - d_0)^\alpha$. The fit parameters are $a = 17.4$ and $d_0 = -9.9$ for the simulation (black dashed line) and $a = 23.5$ and $d_0 = -47.4$ for the experiment (black solid line). We obtain the same value for the exponent, namely, $\alpha \approx -0.69$ in both cases. In the main plot we confirm that, by rescaling the slope data of the experiment and the simulation and plotting $S^* = S/a$ against $d^* = d - d_0$, both curves can be collapsed onto a single power-law (a straight line in log-log plot) with exponent $\alpha \approx -0.69$ (black solid line). Red stars indicate the rescaled values of the simulation and black circles are used for the rescaled experimental data. We also show that the slope of the Panhandle region of the Okavango delta (blue squares) follows a similar behavior.

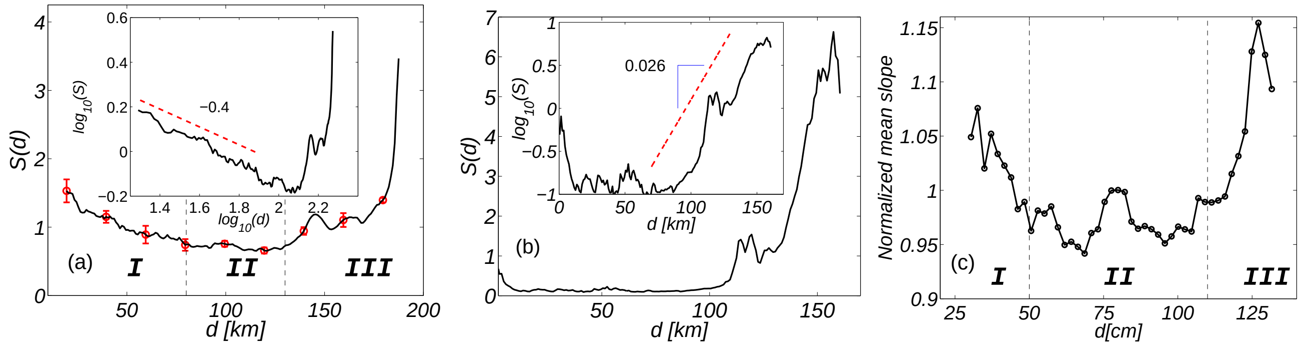

Figure 4. Plot of the slope $S(d)$ from Eq. 5 for wet deltas: Simulation (a), the Mississippi (b) and the wet experiment (c). The average slope for wet deltas is different from that of dry deltas in Fig. 2. Simulation and experiment show an initial part with deceasing slope (I) where the stream adjusts the inclination to its transport capacity followed by a part of almost constant slope with free flow (II) and a strongly increasing part at the head of the delta (III). The inset of the simulation (a) shows that the initial slope decreases like a power law with exponent $\alpha \approx -0.4$. In the real DEM data (b) the Mississippi already adjusted its fluvially accessible area in the coastal plain to its transport capacity and we observe a constant slope at the beginning and an exponentially increasing slope at the end (inset).